Gene Therapy in Patient-specific Stem Cell Lines and a Preclinical Model of Retinitis Pigmentosa With Membrane Frizzled-related Protein Defects

Yao Li[1], Wen-Hsuan Wu[1], Chun-Wei Hsu[1], Huy V Nguyen[2], Yi-Ting Tsai[1], Lawrence Chan[1], Takayuki Nagasaki[1], Irene H Maumenee[3], Lawrence A Yannuzzi[1], Quan V Hoang[1,4], Haiqing Hua[5,6], Dieter Egli[6] and Stephen H Tsang[4,7]

[1]Barbara and Donald Jonas Laboratory of Stem Cells and Regenerative Medicine, and Bernard and Shirlee Brown Glaucoma Laboratory, Department of Ophthalmology, Columbia University, New York, New York, USA; [2]Columbia University College of Physicians and Surgeons, New York, New York, USA; [3]Illinois Eye and Ear Infirmary, University of Illinois at Chicago, Chicago, Illinois, USA; [4]New York-Presbyterian Hospital/Columbia University Medical Center, New York, New York, USA; [5]Division of Molecular Genetics, Department of Pediatrics and Naomi Berrie Diabetes Center, Columbia University, New York, New York, USA; [6]New York Stem Cell Foundation, New York, New York, USA; [7]Department of Pathology and Cell Biology, Columbia University, New York, New York, USA

Defects in Membrane Frizzled-related Protein (MFRP) cause autosomal recessive retinitis pigmentosa (RP). *MFRP* codes for a retinal pigment epithelium (RPE)-specific membrane receptor of unknown function. In patient-specific induced pluripotent stem (iPS)-derived RPE cells, precise levels of MFRP, and its dicistronic partner CTRP5, are critical to the regulation of actin organization. Overexpression of CTRP5 in naïve human RPE cells phenocopied behavior of *MFRP*-deficient patient RPE (iPS-RPE) cells. AAV8 (Y733F) vector expressing human *MFRP* rescued the actin disorganization phenotype and restored apical microvilli in patient-specific iPS-RPE cell lines. As a result, AAV-treated *MFRP* mutant iPS-RPE recovered pigmentation and transepithelial resistance. The efficacy of AAV-mediated gene therapy was also evaluated in *Mfrp*^{rd6}/*Mfrp*^{rd6} mice—an established preclinical model of RP—and long-term improvement in visual function was observed in AAV-*Mfrp*-treated mice. This report is the first to indicate the successful use of human iPS-RPE cells as a recipient for gene therapy. The observed favorable response to gene therapy in both patient-specific cell lines, and the *Mfrp*^{rd6}/*Mfrp*^{rd6} preclinical model suggests that this form of degeneration caused by *MFRP* mutations is a potential target for interventional trials.

Received 1 September 2013; accepted 23 May 2014; advance online publication 8 July 2014. doi:10.1038/mt.2014.100

INTRODUCTION

Induced pluripotent stem (iPS) cells reprogrammed from somatic cells have allowed for the generation of patient-specific disease cells *in vitro*. Interest in generating human-induced pluripotent stem (hiPS) cells for stem cell modeling of diseases has overtaken that of patient-specific human embryonic stem cells due to the ethical, technical, and political concerns associated with the latter. As a platform to study patient-specific targeted disease cells, hiPS cells have exciting potential in regenerative medicine and human disease modeling. The *in vitro* phenotype of disease-specific iPS-derived cells can be used to bridge the knowledge gap between the clinical phenotype and molecular or cellular mechanisms, along with further applications, such as creating new strategies for drug screening or developing novel therapeutic agents.[1] By using hiPS cells, we can prove that a disease is caused by a gene mutation and hypothesize potential treatment options before using more expensive animal studies.[2] The hiPS cell-based disease models may also assist in the development of novel treatments for clinical trials.[3–5]

Retinitis pigmentosa (RP), which affects approximately 1.5 million people worldwide, can have autosomal dominant, autosomal recessive, or X-linked inheritance patterns. To date, over 60 genes have been linked to the autosomal and X-linked forms of RP, of which over half (35) are associated with the recessive pattern of inheritance. One such discovered gene is *Mfrp* (MIM 606227), which encodes a retinal pigment epithelium (RPE)-specific membrane receptor of unknown function.[6,7] The *MFRP* gene encodes a type II transmembrane protein similar to WNT-binding frizzled proteins. This protein is encoded in a dicistronic transcript, which also contains the complete open reading frame (ORF) of the complement C1q tumor necrosis factor-related protein-5 (C1QTNF5/CTRP5) (MIM 608752) in the 3'-untranslated region.[8,9] MFRP and CTRP5 colocalize on within the RPE and ciliary bodies and interact directly with each other.[7,9–11] MFRP and CTRP5 are thought to exist in an antagonistic relationship,[7,9,10,12] but there is no direct proof published at this time.

Mfrp^{rd6}/*Mfrp*^{rd6} mice have a 4-base pair (bp) deletion in the splice donor sequence on intron 4. The subsequent absence of exon 4 causes a deletion of 58 amino acids in the MFRP protein.[9] These mice have autosomal recessive, progressive retinal degeneration, which is evident from white spotting visualized during fundus examination. As a result, these mice lose photoreceptors with age. Histological analysis

Wen-Hsuan Wu, Chun-Wei Hsu and Huy V. Nguyen contributed equally to this work

Correspondence: *Stephen H Tsang, Edward Harkness Eye Institute, 160 Fort Washington Avenue, Research Annex, Room 513, New York, New York 10032, USA. E-mail: sht2@columbia.edu*

shows that the 12–14 cell layers found at birth decline to 4–5 layers by 4.5 months, 2–4 layers by 7 months, and 1 layer by 24 months. Beginning at 1 month, rod and cone photoreceptor function is progressively lost, and function is completely absent by 70 weeks.[9] As a preclinical model of RP, $Mfrp^{rd6}/Mfrp^{rd6}$ mice are ideal recipients to test *in vivo* treatment for RP caused by MFRP deficiency.

For human genetic diseases, uncovering the relationship between functionally related proteins is a step toward further understanding the mechanisms of disease and potential treatment. The goal of this study is to use hiPS cell technology to elucidate the role of a novel mutation in the *MFRP* gene and its putative association with RP. Modeling pathogenesis and treatment *in vitro* using patient-specific iPS cells will help to decrease patient risk, clarify disease mechanisms, bypass problems related to differences among species that arise when using animal models, and reduce the cost of clinical trials. In this study, we generated iPS cells from two RP patients with *MFRP* mutations, treated their iPS-RPE cells with AAV vector therapy, and used their iPS-RPE cells to identify MFRP downstream targets.

RESULTS

Retinitis pigmentosa due to MFRP deficiency

RP in a 19-year-old man (Patient 1, P1) and a 50-year-old woman (Patient 2, P2) was diagnosed by the coauthors (SHT, IHM, QVH, and LAY). P1 showed a relative preservation of his retina compared to other forms of RP (**Figure 1a**). He did not exhibit significant loss of the photoreceptor nuclear layer but had cystic degeneration of the macula seen on optical coherence tomograms (OCT) (**Figure 1e**). Full-field electroretinogram (ERG) analysis of P1 showed extinguished scotopic rod-specific amplitudes but relative sparing of cone responses (**Figure 1f**). P2 showed macular atrophy and extensive subretinal salt-and-pepper RPE mottling (**Figure 1b**). DNA sequencing of *MFRP* revealed that P1 carried a novel homozygous IVS10 +5G>A mutation in the *MFRP* gene (**Figure 1c**). We confirmed this mutation by DNA sequencing of the *MFRP* gene on parents of P1, and both of the parents were heterozygous IVS10 +5G/A (**Supplementary Figure S1**). P2 carried a homozygous, 1-bp del (492C mutation) in the *MFRP* gene (**Figure 1d**).

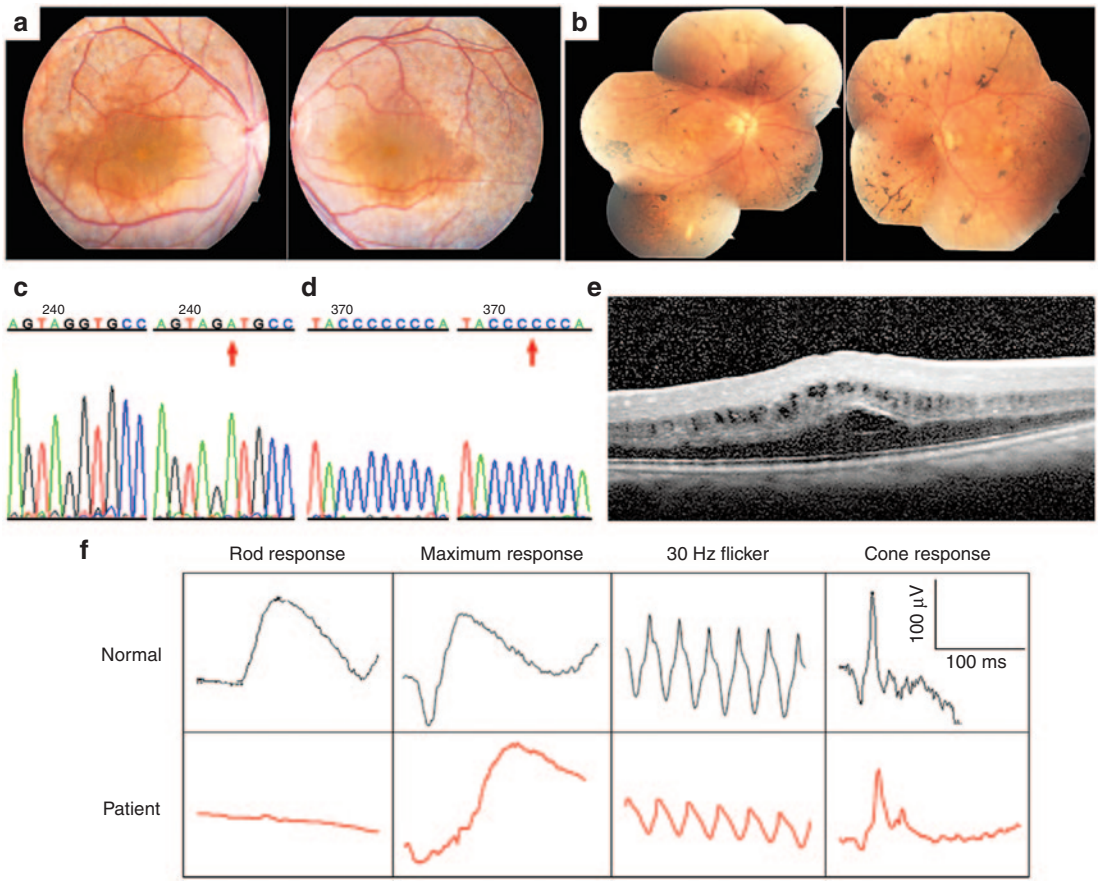

Figure 1 Fundus examination of two *MFRP*-mutant patients. (**a**) Color fundus photographs from Patient 1, P1. OD (right eye) (left picture) and OS (left eye) (right picture) show relative preservation of the retina compared to other forms of RP. (**b**) Fundi from Patient 2, P2, OD (left picture) and OS (right picture) show typical para-arterial intraretinal migration, macular atrophy, and extensive subretinal salt-and-pepper RPE mottling. (**c**) Partial electropherogram of IVS10 of the *MFRP* gene with the normal sequence (left) and a G-A +5 mutation (pointed by red arrow) in P1 (right). (**d**) Partial electropherogram of exon 5 in the *MFRP* gene with the normal sequence (left) and a homozygous 1-bp del (492C) (pointed by red arrow) in P2 (right). (**e**) Optical coherence tomography (OCT) of the macula in P1 shows cystic degeneration and thickening of the foveal region. (**f**) Full-field electroretinogram (ERG) analysis of P1 shows extinguished scotopic rod-specific amplitudes but relative sparing of cone responses.

Patient-specific cell lines

Fibroblast cells from skin samples of P1 and P2 were transduced with lentiviruses carrying the reprogramming genes *OCT4*, *SOX2*, *c-MYC*, and *KLF4* to establish patient-specific iPS cell lines; fibroblasts from a healthy donor's biopsy sample (female, 56-year-old) were also cultured and reprogrammed in the same way to generate a wild-type control iPS line. Immunocytochemistry analysis, followed by confocal microscopy, demonstrated that all undifferentiated iPS lines expressed the pluripotent markers Oct-4, Sox-2, SSEA4, TRA-1-60, and NANOG (**Figure 2a**). Teratoma assays confirmed the pluripotency of each iPS line (**Supplementary Figure S2**).

Following differentiation, pigment clusters derived from iPS cells appeared after 6–8 weeks. Under light microscope, the wild-type control iPS-RPE showed native RPE morphological characteristics, including perinuclear localization of melanin granules. In contrast, iPS-RPE cells from both P1 and P2 had abnormal morphology with less pigment, mislocalized pigment distribution, and loss of clear cellular boundaries and cell-to-cell contact (**Figure 2b**). Immunoblot analyses for the native, mature RPE-specific markers RPE65, BESTROPHIN-1, MITF, and VINCULIN confirmed the RPE fate of iPS-RPE cells from wild-type control, P1 and P2 (**Figure 2c**, quantification shown in **Supplementary Figure S3**).

AAV2/8(Y733F) gene therapy vectors

The AAV2/8(Y733F)-CMV gene transfer vector[13–15] was based on pZac2.1. *MFRP*, *CTRP5*, or *Mfrp* cDNA was cloned into this expression cassette along with the CMV promoter, a Simian virus 40 (SV40) site, and a polyA tail flanked by inverted terminal repeats (ITRs) (**Figure 3**). In this report, the AAV2/8(Y733F).CMV.hu*MFRP*.SV40 vector will be referred to as AAV-*MFRP*, the AAV2/8(Y733F).CMV.hu*CTRP5*.SV40 vector will be referred to as AAV-*CTRP5*, and the AAV2/8(Y733F).CMV.m*Mfrp*.SV40 vector will be referred to as AAV-*Mfrp*.

Label-free mass spectrometric proteome profiling

Label-free shotgun proteomic profiling provided data to identify key proteins from thousands of proteins and discern differences in protein expression phenotypes across cell lines with various genotypes.[16] β-actin emerged as the most significant differentially-expressed protein in iPS-RPE lines derived from our two *MFRP*-mutant patients; its level was two-fold higher compared to wild-type control iPS-RPE. No other protein in the dataset had this striking pattern of expression β-actin as a candidate in MFRP signaling pathway. Immunoblot analyses confirmed the results from the proteomic profiling: similar patterns were observed in β-actin expression (**Figure 4a**), with increased level in iPS-RPE derived from our two *MFRP*-mutant patients compared to wild-type control iPS-RPE.

MFRP level is inversely proportional to CTRP5 expression in RPE cells

To explore the relationship between MFRP and CTRP5 in RPE cells, antibodies to MFRP and CTRP5 were used to probe extracts from iPS-RPE, human autopsy RPE, and AAV-*MFRP*-transduced

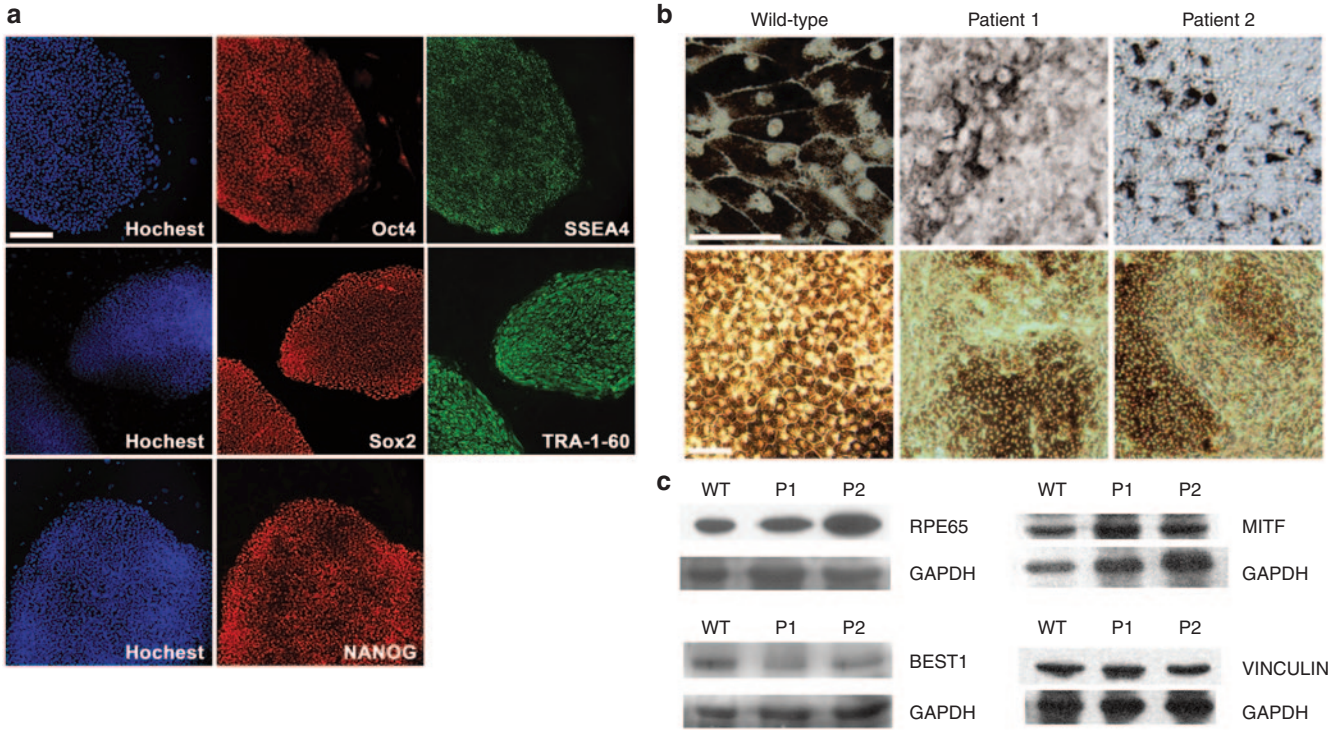

Figure 2 Establish patient-specific cell lines. (**a**) Representative immunofluorescence image of pluripotency markers in established patient-specific iPS cell line. Scale bar: 100 µm. (**b**) Light microscopy images of cultured human iPS-RPE cells from a wild-type control donor (left), P1 (middle), and P2 (right). For upper panel, scale bar: 50 µm; lower panel, scale bar: 100 µm. **(c)** Immunoblot analysis of mature RPE specific marker RPE65 (65 kDa), BESTROPHIN-1 (68 kDa), MITF (59kDa), and VINCULIN (124 kDa) in iPS-RPE cells from wild-type control donor (WT), P1, and P2. GAPDH serves as the loading control.

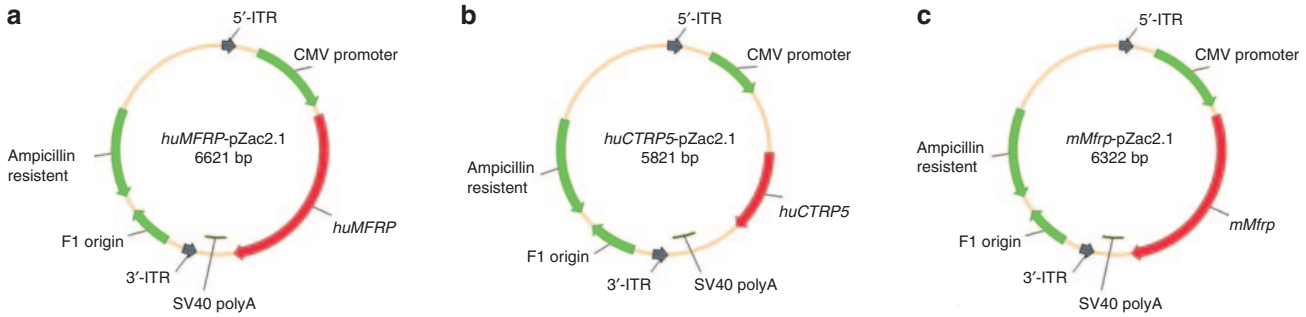

Figure 3 Schematic representation of the AAV2/8(Y733F)-CMV-vector. A pZac2.1 vector plasmid displaying the complementary DNA (cDNA) of human *MFRP*. (**a**), human *CTRP5* (**b**), and mouse *Mfrp* (**c**) fragments driven by the CMV promoter. The Simian virus 40 (SV40) polyadenylation signal is located at the 3′ end of the cDNA. Arrows indicate the direction of transcription, and the 5′- and 3′-inverted terminal repeat (ITRs) of AAV are shown.

HEK293 cells. Immunoblotting results presented that *MFRP* and its dicistronic gene *CTRP5* existed in an antagonistic relationship to regulate actin organization. Lack of *MFRP* expression with corresponding increases in CTRP5 and β-actin levels were observed in iPS-RPE cells derived from both P1 and P2 compared to wild-type control iPS-RPE. When naive human RPE cells, isolated from an autopsied eye, were transduced with AAV-*CTRP5*, a decrease in the MFRP and increase in CTRP5 and β-actin levels was observed compared to nontransduced controls. Strong MFRP expression and null CTRP5 expression was observed in HEK293 cells transduced with AAV-*MFRP*, which served as a positive control for AAV-mediated transgene expression, despite loading at 20% concentration compared to the RPE experiments. In all lanes, CTRP5 expression opposed MFRP expression. Mature RPE fates were further confirmed by the expression of RPE-specific protein, CRALBP, in all iPS-RPE cells and autopsied RPE, yet not in HEK293 cells. The RPE from an autopsied eye with nontreated and wild-type control iPS-RPE cells served as the positive control (**Figure 4a**, quantification shown in **Supplementary Figures S3** and **S4**).

Overexpression of CTRP5 phenocopies the MFRP deficiency

In immunoblots, overexpression of CTRP5 led to down-regulation of MFRP in AAV-*CTRP5* transduced human autopsy RPE cells. To confirm the relationship between MFRP and CTRP5, immunofluorescence for rhodamine-phalloidin was performed on the wild-type control iPS-RPE, MFRP-deficient iPS-RPE (P1), and human autopsy RPE before and after AAV-*CTRP5* treatment. Under fluorescence microscopy, the wild-type control iPS-RPE and nontreated human autopsy RPE showed similar morphology: organized actin filaments arranged in dense bands around the cell periphery and actin stress fibers extending throughout the cytoplasm. Both iPS-RPE cells from P1 and AAV-*CTRP5* transduced human autopsy RPE showed disorganized and elongated crisscrossing actin stress fibers, increased numbers of focal adhesions, and loss of cell-to-cell contact (**Figure 4b**).

AAV-*MFRP* gene therapy rescues dysmorphic MFRP-deficient iPS-RPE cells

iPS-RPE cells from the two *MFRP* mutant patients and the *Mfrp*^{rd6}/*Mfrp*^{rd6} mouse were found to be pleiotropic compared to the hexagonal RPE cells derived from wild-type control iPS-RPE and C57BL/6(B6) mice controls. Flat mount of RPE immunolabeled for tight-junction zonula occludens (ZO-1) protein from a *Mfrp*^{rd6}/*Mfrp*^{rd6} mouse shows marked variation in cell size compared to the RPE from adult B6 mice, which served as controls (**Figure 5a**). In iPS-RPE, the hexagonal red structure indicates the presence of ZO-1 on wild-type control iPS-RPE cells. Cellular morphology is lost in iPS-RPE cells from P1 and P2, but the regular hexagonal pattern of ZO-1 expression was restored in dysmorphic iPS-RPE cells from P1 and P2 following AAV-*MFRP* vector treatment (**Figure 5b**). Microfilament organization of RPE cells was assessed by immunofluorescence analysis with rhodamine-phalloidin staining. Wild-type iPS-RPE shows precisely organized β-actin filaments arranged in dense bands around the cell periphery with short actin stress fibers extending throughout the cytoplasm. MFRP-deficient iPS-RPE from P1 and P2 exhibit elongated crisscrossing actin stress fibers, increased numbers of focal adhesions, and loss of cell-cell contact. AAV-*MFRP* treatment restored actin filament bundle organization to the iPS-RPE from P1 and P2. After AAV-*MFRP* treatment, iPS-RPE cells from P1 and P2 exhibited hexagonal, organized actin filaments around the cell periphery (**Figure 5c**).

Supernumerary microvilli were observed in *Mfrp*^{rd6}/*Mfrp*^{rd6} mice.[17] However, human iPS-RPE cells from P1 and P2 showed a loss of apical microvilli, which was restored after AAV-*MFRP* treatment (**Figure 6**). Wild-type iPS-RPE cells were used as a control.

In trans-well culture system, wild-type control iPS-RPE cells exhibit strong pigmentation whereas the iPS-RPE from P1 and P2 showed significant loss of pigment. Strikingly, after AAV-*MFRP* transduction, *MFRP*-mutant iPS-RPE cells regained pigmentation (**Figure 7a**).

Patients with MFRP deficiency lost the RPE barrier function and developed cystic degeneration in their maculae (**Figure 1e**). Transepithelial resistance (TER) reveals the status of RPE tight junctions. In order to quantify the functional impact of AAV-*MFRP* rescue, we used TER to reveal the status of tight junctions between iPS-RPE cells treated with and without AAV-*MFRP*. TER in the wild-type control iPS-RPE increased to 320Ω cm^{-2} over 5 weeks. The iPS-RPE from both P1 and P2 showed a significant improvement (P value = 0.0001183 for P1, and P value = 0.000341 for P2) at all weeks tested for cells transduced with

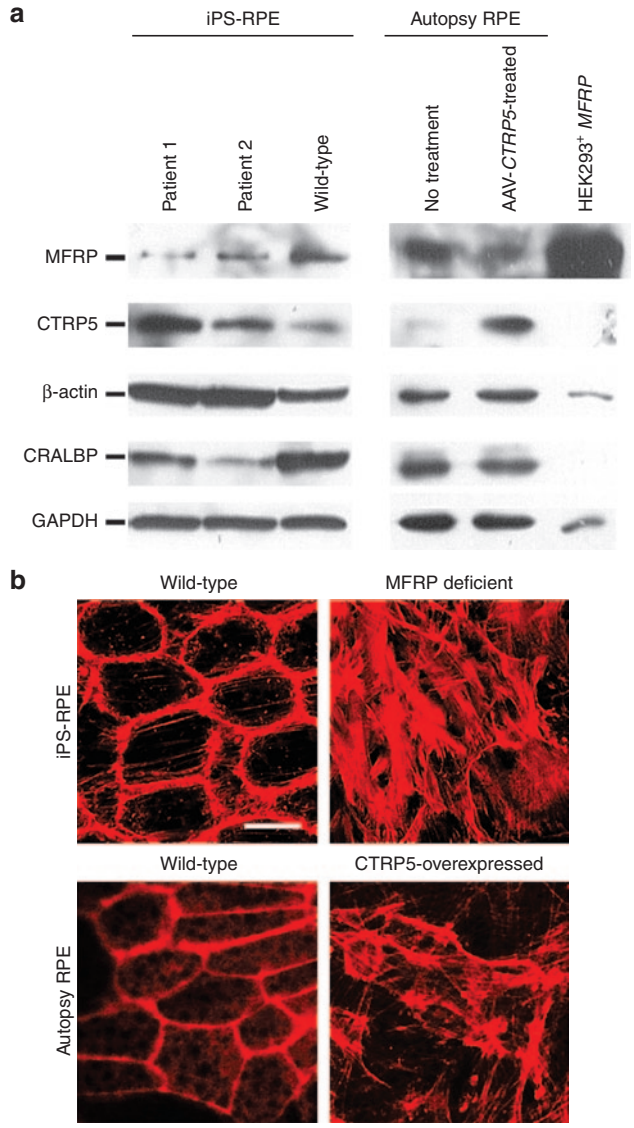

Figure 4 Immunoblots and immunofluorescence on MFRP-deficient and CTRP5-overexpressed RPE cells. (**a**) Antibodies to MFRP, CTRP5, β-actin, CRALBP (RPE-specific marker), and GAPDH were used to probe extracts from iPS-RPE from P1, P2 and the wild-type control donor (lanes 1-3), autopsy RPE without and with AAV-*CTRP5*-treated (lanes 4-5), and HEK293 cells transduced with AAV-*MFRP* (lane 6). (**b**) Immunofluorescence for rhodamine-phalloidin on wild-type iPS-RPE cells (upper left), MFRP-deficient iPS-RPE cells from P1 (upper right), human autopsy RPE (bottom left) and human autopsy RPE treated with AAV-*CTRP5* vector (bottom right). Scale bar = 10 µm.

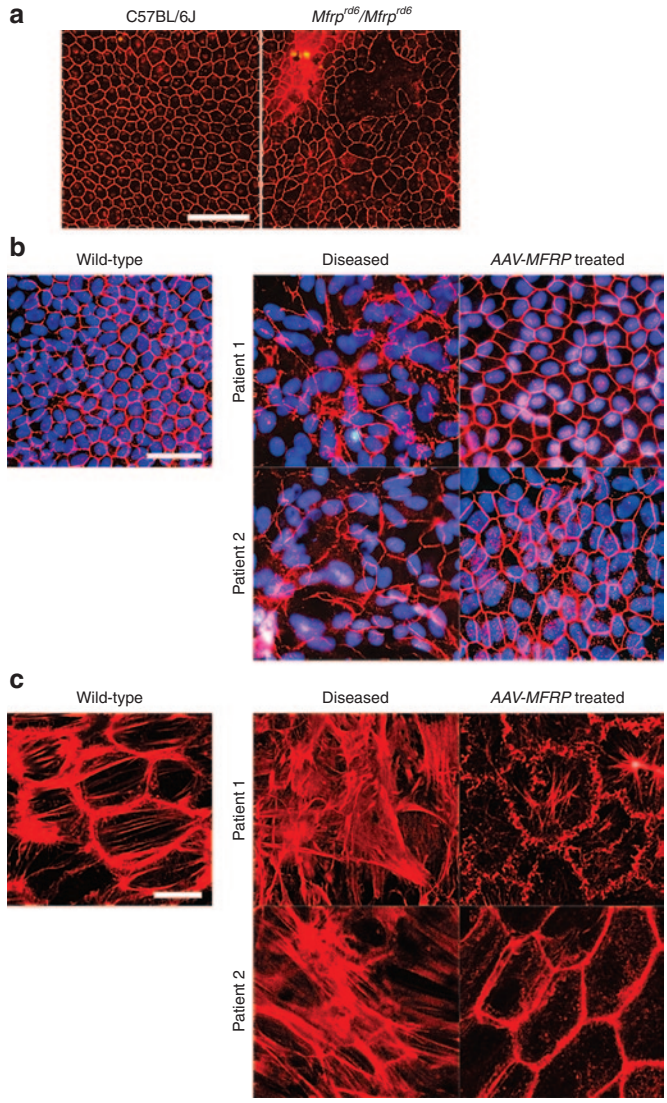

Figure 5 Immunofluorescence on RPE without and with AAV-*MFRP* treated. (**a**) A flat mount of a RPE sheet immunolabeled for tight-junction protein ZO-1 from C57BL/6 (B6) mice (left), serve as control and an $Mfrp^{rd6}/Mfrp^{rd6}$ mouse (right). Scale bar: 100 µm. (**b**) Immunofluorescence staining for ZO-1 (red) and nuclear DAPI staining (blue) on iPS-RPE monolayer from wild-type control donor, P1, P2, and iPS-RPE from P1 and P2 after AAV-*MFRP* treatment. Scale bar: 50 µm. (**c**) Rhodamine-phalloidin immunofluorescence to assess microfilament organization on iPS-RPE cells from control donor, P1, P2, and iPS-RPE from P1 and P2 after AAV-*MFRP* treatment. Scale bar: 10 µm.

the AAV-*MFRP* vector compared to untreated cells. The TER at 5 weeks for the AAV-transduced group reached 64 Ω cm^{-2} for P1 and 70 Ω cm^{-2} for P2 (**Figure 7b**).

AAV-*Mfrp* provides long-term vision rescue in a preclinical model of RP

Quantitative autofluorescence (AF) images in $Mfrp^{rd6}/Mfrp^{rd6}$ mice showed an increase in punctate and general lipofuscin accumulation at 30, 60, and 90 days of age (**Figure 8a**). To prevent photoreceptor cell death in $Mfrp^{rd6}/Mfrp^{rd6}$ mice, the right eyes were transduced by subretinal injection of the AAV-*Mfrp* vector on postnatal day 5. Compared to the control left eyes of the $Mfrp^{rd6}/Mfrp^{rd6}$ mice, AAV-*Mfrp* transduction decreased background AF and resulted in fewer punctate signals in the treated eye (**Figure 8b**). Quantification of AF showed a significantly decreased AF from a density–volume of 137.01 to 43.59 (*P* value = 0.02) (**Figure 8c**). Composite dark-adapted electroretinograms (ERGs), which served as a direct proof of retina function, were performed two months after unilateral subretinal injection of wild-type *Mfrp* via the AAV-*Mfrp* vector. The other eye served as the untreated control. Rod-specific response and maximum response ERGs were recorded for 11 mice. The function of both rod and cone photoreceptors increased significantly, as evidenced by an increased amplitude of the a-wave

(from −42.23 to −143 μv) and b-wave (from 182.7 to 343.8 μv) (**Figure 8d**). Retinal histology of *Mfrp*^{rd6}/*Mfrp*^{rd6} mutant retina and AAV-*MFRP*-transduced retina presented an increased outer nuclear layer (ONL) from a thickness of 4-5 nuclei to a thickness of 7–8 nuclei ($P = 0.0035$) (**Figure 8e,f**). The rescued photoreceptors showed improved function and survival for at least 6 months. The retina sections of AAV2/8(Y733F)-m*Mfrp*-treated *Mfrp*^{rd6}/*Mfrp*^{rd6} mice showed a clear layer of RPE-specific expression, whereas non-treated *Mfrp*^{rd6}/*Mfrp*^{rd6} mice did not (**Figure 8g**). Together, these data indicate favorable response to gene therapy in both *Mfrp*^{rd6}/*Mfrp*^{rd6} preclinical model and patient-specific cells.

DISCUSSION

Human iPS cell technology provides a platform for investigating the pathophysiological mechanisms of genetic mutations and testing of gene therapy vectors. In this study, we described a human iPS cell model of MFRP-deficient RP that possessed functional deficiencies consistent with the clinicopathological features of the disease.[10,11,15] Focusing on an RPE-based disease model presents several advantages. iPS-RPE can be reproducibly isolated and closely monitored both morphologically and functionally before experiments, effectively minimizing variability in the timing of differentiation. In addition, the RPE, unlike many other human cell types, has a well-described culture standard, ensuring proper controls.[18,19]

Our study accomplished four objectives. First, it described the successful characterization of human-derived iPS cells from two RP patients, one of them with a novel mutation in the *MFRP* gene, homozygous IVS10 +5G>A, which had never been reported before. Second, it demonstrated that iPS-derived cells could be used as surrogate endpoints for FDA trials and a platform for *in vitro* testing of AAV vectors. Third, this study identified actin organization as a downstream target of MFRP and demonstrated a new putative function of this novel gene related to cytoskeleton organization. Fourth, this study expounded upon the inverse relationship between MFRP and CTRP5 in human RPE cells.

Traditionally, human genetic diseases were modeled in mice, but here, we showed that patient-specific cells and a mouse model did not have the same phenotype. Compared to RPE derived from wild-type control iPS cells, iPS-RPE from our *MFRP* patients exhibited the loss of apical microvilli as observed by electron microscopy (**Figure 6**). This result was in stark contrast to the phenotype of the RPE in *Mfrp*^{rd6}/*Mfrp*^{rd6} mice, which showed higher densities of apical microvilli.[17] Because differences in phenotypic expression can be observed among species with the same genetic

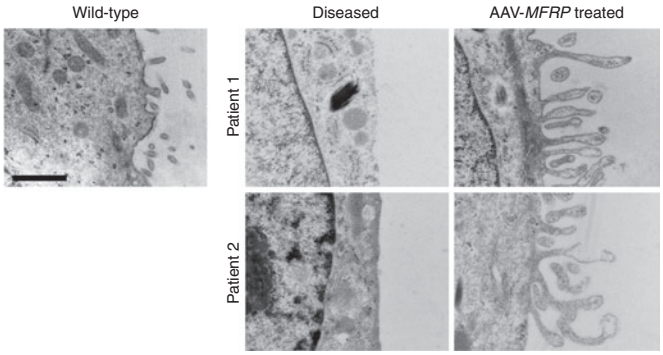

Figure 6 Transmission electron microscopy of microvilli in patient-specific iPS-RPE without and with AAV-*MFRP* treatment. AAV-MFRP treated RPE regain lost microvilli. Scale bar: 1 μm.

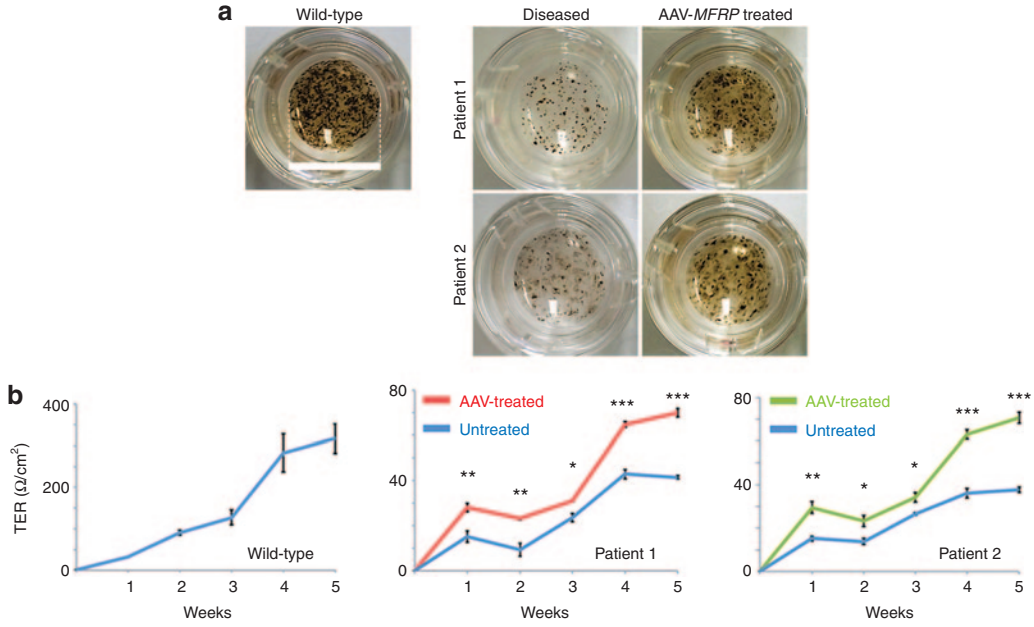

Figure 7 Transepithelial resistance assessment of patient-specific iPS-derived RPE within and without AAV-*MFRP* treatment. (**a**) Representative images of patient-specific iPS- RPE in trans-well plate without and with AAV-*MFRP* treatment (one of four replicate wells for each iPS-RPE line is shown). Scale bar: 1.5 cm. (**b**) Transepithelial resistance (TER) in the wild-type control iPS-RPE increased to 320 Ω cm^{-2} over 5 weeks. The iPS-RPE cells from P1 and P2 treated with the AAV-*MFRP* show a significant improvement TER (*$P < 0.05$, **$P < 0.01$, or ***$P < 0.001$) at all tested time points compared to untreated cells. The TER at 5 weeks for the AAV-*MFRP* treated group reached 64 Ω cm^{-2} for P1 (P value = 0.0001183) and 70 Ω cm^{-2} for P2 (P value = 0.000341).

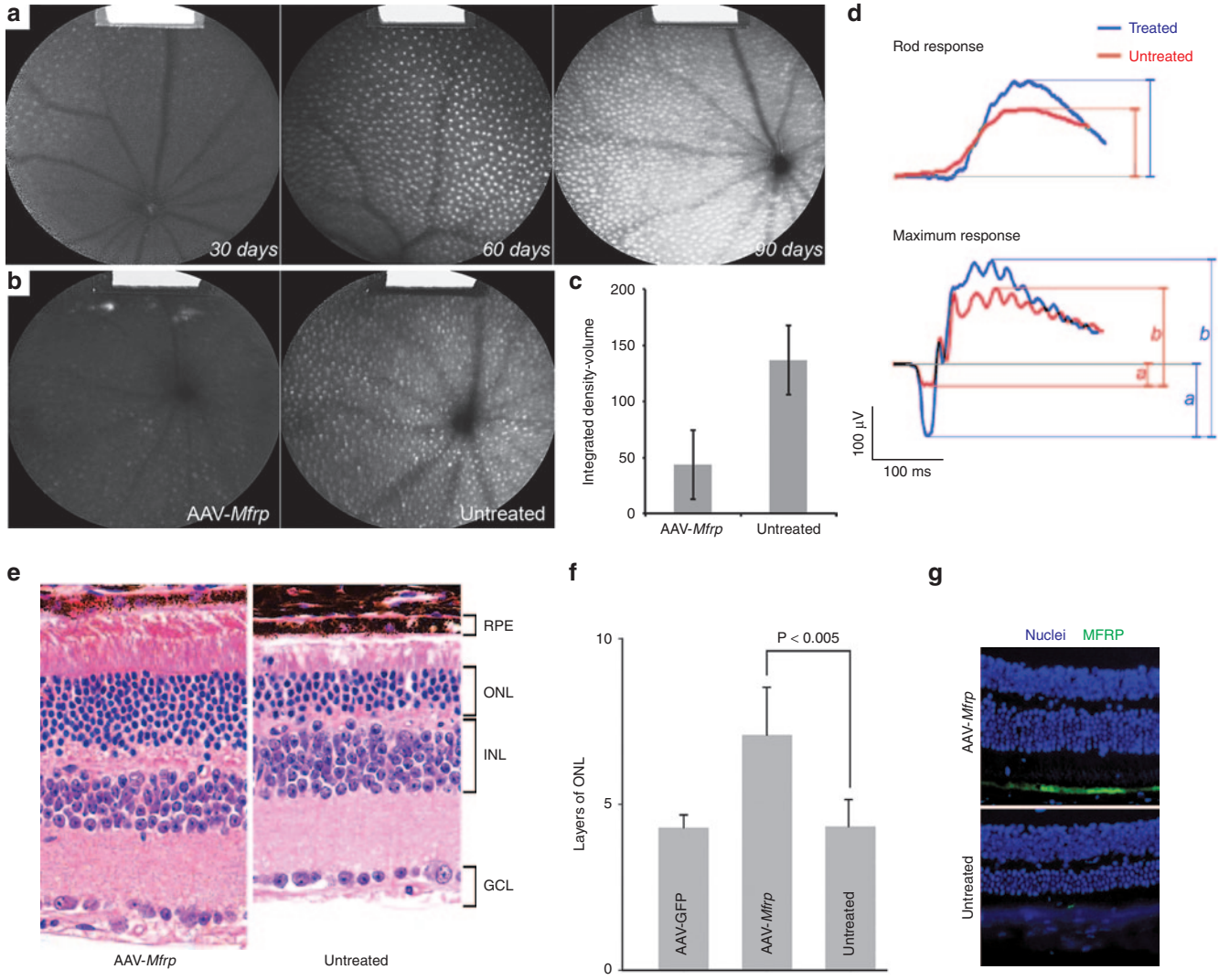

Figure 8 AAV-*Mfrp* treatment on *Mfrp*^{rd6}/*Mfrp*^{rd6} mice. (**a**) Quantitative AF images in *Mfrp*^{rd6}/*Mfrp*^{rd6} mice at 30, 60, and 90 days of age. (**b**) Retinal fundus AF images of the untreated left eye (left) and the AAV-*Mfrp*-treated right eye (right) in *Mfrp*^{rd6}/*Mfrp*^{rd6} mice. A fluorescence standard, shown as a bright strip at the top of each image, enabled intensity comparison. (**c**) Graphical quantification of AF level in treated and nontreated eyes ($P = 0.02$). (**d**) Rod-specific response and maximum response electroretinograms (ERGs) recordings from 11 *Mfrp*^{rd6}/*Mfrp*^{rd6} mice that received AAV-*Mfrp* subretinal injection in right eye at 60 days after the transplantation surgery. Amplitudes of a-wave (**) indicated by letter "a" and b-wave (*) indicated by letter "b". **(e)** Retinal histology (Hematoxylin and eosin staining) of a representative *Mfrp*^{rd6}/*Mfrp*^{rd6} mutant retina (right panel) and AAV-*MFRP* transduced retina (left panel). GCL, ganglion cell layer; INL, inner nuclear layer; ONL, outer nuclear layer. (**f**) Quantification of ONL of AAV-GFP treated, AAV-*Mfrp* treated and nontreat eyes in *Mfrp*^{rd6}/*Mfrp*^{rd6} mice. (**g**) Representative immunofluorescence pictures of retina histology sections stained by anti-mouse MFRP from AAV-*Mfrp*-treated eye (top) and non-treated eye (bottom) of *Mfrp*^{rd6}/*Mfrp*^{rd6} mice.

mutation, a study of patient-specific cell lines can be complementary to mouse models.

The RPE dysmorphology suggested that patient specific RPE cells may be more developmentally delayed. Defective MFRP in both patients and *Mfrp*^{rd6}/*Mfrp*^{rd6}mice affects proper axial length development. To define the biochemical basis of dysmorphic RPE, we applied an unbiased proteome screen and identified actin via mass spectrometry as a potential protein involved in the MFRP pathophysiological pathway (all Excel data provided in **Supplementary Table S1**). To validate the mass spectrometry results, we used immunoblots to test the protein with significant up or downregulated status. In all MFRP-deficient and CTRP5-overexpressed RPE lines, β-actin was twofold higher than those wild-type controls. To further confirm the immunoblotting results, we performed rhodamine-phalloidin and found that MFRP-deficient iPS-RPE exhibited increased β-actin expression and altered actin polymerization in cellular level compared to wild-type control iPS-RPE (**Figure 5**). These results reinforce our novel hypothesis that actin polymerization is a downstream effect in the MFRP signaling.

The *CTRP5* gene is a dicistronic partner of *MFRP*, and its secreted protein, CTRP5, has been shown to bind to MFRP.[20,21] MFRP and CTRP5 proteins share the functionally related CUB and C1q domains. In prokaryotes, polycistronic transcripts commonly encode proteins in the same functional pathway, thus constituting an operon. Studies have shown that several dicistronic transcripts exist in mammals, and most of these genes encode functionally related proteins. As we mentioned, defects in *MFRP*

cause autosomal recessive RP. Likewise, the S163R mutation in the *CTRP5* causes late-onset retinal macular degeneration (LORD), an autosomal dominant condition in humans that closely resembles age-related macular degeneration (AMD).[22,23] Secretion of CTRP5 into the extracellular matrix is impaired by the S163R mutation, causing an unfolded protein response within the endoplasmic reticulum (ER).[20] The heterozygous *CTRP5* knock-in mouse model (*Ctrp5*$^{+/S163R}$), similarly as *Mfrp*^{rd6}/*Mfrp*^{rd6} mice, also develop RPE abnormalities, early dark adaptation abnormalities, accumulation of hyperautofluorescence spots, drusen, Bruch membrane abnormalities, and loss of photoreceptors.[8,23,24]

Like other dicistronic genes, *MFRP* and *CTRP5* may participate in a common biological pathway in RPE, but no functional relationship between *MFRP* and *CTRP5* has been proposed. Several studies have confirmed that *CTRP5* is a binding partner of *MFRP*,[7,9,10,12] but here, we provided evidence for an inverse relationship between these two binding partners. Expression of *MFRP* in iPS-RPE derived from our two *MFRP*-mutant patients is lower compared to wild-type controls. Additionally, CTRP5 levels are higher in MFRP-deficient iPS-RPE cells compared to wild-type controls. To validate this finding, we transduced AAV-*CTRP5* into native RPE cells from an autopsy human eye. After two weeks, we measured the expression level of *MFRP* and *CTRP5* in treated and nontreated RPE cells. In AAV-*CTRP5*-transduced RPE cells, increased CTRP5 expression led to low *MFRP* levels. In different independent RPE lines, CTRP5 levels are inversely proportional *MFRP* levels.

Besides the expression level, we tested the hypothesis that *MFRP* and *CTRP5* play the same functional role in RPE cells. From the result of immunoblots, increased β-actin levels were observed in both *MFRP*-deficient RPE cells and *CTRP5*-overexpressed RPE cells. We used rhodamine-phalloidin staining to monitor β-actin level in these RPE cell lines and found that overexpression of CTRP5 presented similar cellular phenotype as the *MFRP* deficiency (**Figure 4b**). We also transduced AAV-*CTRP5* into wild-type control iPS-RPE, and also obtained a similar result (images of autopsy RPE and wild-type iPS-RPE transduced by AAV-GFP alone as negative control were also included in **Supplementary Figure S5**).

In this report, we presented an expeditious system for the study of a new disease allele using iPS cell technology. By creating a patient-specific model of the disease via iPS, we could study the phenotypic properties of the disease and its potential treatments on a virtually unlimited sample of cells. Following our *in vitro* studies, we used a diseased preclinical model to monitor physiological responses to the same AAV treatment *in vivo*. This approach using human iPS cells to study genetic diseases allowed for the efficient testing of gene therapy *in vitro* before studying live models. In this study, we used patient-specific stem cell lines to identify two distinct and novel findings concerning *MFRP* disease: (i) *MFRP* affects downstream actin polymerization, and (ii) *MFRP* coexisted with *CTRP5* in an antagonistic, dose-dependent relationship. While this approach can be used across specialties, it would be particularly important for inherited retinal degenerative diseases, which are often caused by multiple defects and have unclear or unknown disease mechanisms. Patient-specific stem cells represent an incredible resource for gene therapy studies, not only in degenerative disorders of the retina, but also in genetic disorders of other organ systems.

MATERIALS AND METHODS

Research subjects. Color fundus pictures, optical coherence tomography (OCT), and electroretinogram (ERG) analysis were performed on two *MFRP*-related RP patients in the Department of Ophthalmology, Columbia University Medical Center/New York Presbyterian Hospital. Skin biopsy samples were obtained (IRB Protocol AAAF1849) from the two patients and a healthy subject using local anesthesia (lidocaine) and a biopsy-punch (McKesson, VA). The samples were processed and cultured as previously described.[18,25]

The mouse procedures were approved by the Institutional Animal Care and Use Committee of Columbia University. *Mfrp*^{rd6}/*Mfrp*^{rd6} mice were used in accordance with the Statement for the Use of Animals in Ophthalmic and Vision Research of the Association for Research in Vision and Ophthalmology.

MFRP sequencing. Genomic DNA from both patients was isolated from peripheral blood lymphocytes according to standard methods. The entire coding sequence and exon-intron boundaries of *MFRP* (13 exons) were amplified by PCR using pairs of primers that were designed based on the published consensus sequences.[12] Direct sequencing of the PCR-amplified products was analyzed by the Genwize Company (NJ). All *MFRP* exon data are available at Gene Expression Omnibus (MIM 606227).

Generation and maintenance of hiPS cell lines. Primary fibroblasts from two RP patients and one healthy donor were converted into pluripotent stem cells using lentiviruses carrying the reprogramming genes *OCT4*, *SOX2*, *c-MYC*, and *KLF4*, following the previously established protocol. All hiPS lines were maintained in hiPSC medium as previously described.[18,26] All iPS cells were passaged every 3–4 days.

Differentiation of hiPSC lines. iPS differentiation started at passage 9 for all iPS lines in this study. For differentiation, hiPS colonies were cultured as floating clusters in 6-well culture dishes (Costar, Corning, Corning, NY) pretreated with MEFs in knockout medium (KOM) consisting of KO-DMEM, 15% KO serum replacement, 1% nonessential amino acids, 2 mmol/l glutamine, 50 U/ml penicillin, 50 mg/ml streptomycin (all from GIBCO-BRL), and 10 mmol/l nicotinamide (NIC) (Sigma-Aldrich, St Louis, MO).[27] After 6–10 weeks, pigmented clusters were formatted and plated on 1% matrigel-coated dishes in RPE culture medium according to a previous protocol[28] for a characterization assay. To obtain a monolayer for the function assay, after 8 weeks of differentiation, the pigmented areas were isolated manually and plated in 12-well transwell plates (Costar, Corning). RPE cells derived from iPS cells (iPS-RPE) were maintained in MEM (α modification, Sigma-Aldrich, M-4526) -based RPE medium, which contains N1 supplement (5 ml per 500 ml medium), Taurine (125 mg per 500 ml medium), Hydrocortisone (10 μg per 500 ml medium), Triiodo-thyronin (0.0065 μg per 500 ml medium) (all from Sigma-Aldrich), 2 mmol/l glutamine, 50 U/ml penicillin-streptomycin, 1% nonessential amino acids and 10% fetal bovine serum (all from GIBCO-BRL), for 6–8 weeks to allow them to form a functional monolayer and to reproduce pigment.

Human autopsy RPE isolation. Human autopsy RPE cells were isolated and cultured from human eye samples obtained from New York Eye Bank as described previously.[2] In brief, the eyecup, with anterior portions removed, was incubated at 37 °C for 60 minutes. The retina was then separated from the optic nerve. Next, RPE-Bruch's membrane and the combined tissues were separated from the choroid layer and transferred to a 15 ml conical tube containing 0.05% trypsin-EDTA. The conical tube was then incubated in a 37 °C water bath for 10–15 minutes. After centrifugation at 1.4 rpm for 4 minutes, the pellet was then resuspended in RPE medium and plated on a petri dish.

Construction of AAV vectors. AAV serotype 2/8 capsids, which contain a point mutation in the surface-exposed tyrosine residue AAV2/8(Y733F), were used for packaging the human *MFRP*, human *CTRP5*, and mouse *Mfrp* constructs. Vector plasmids were constructed by inserting the CMV promoter region and the full-length *MFRP*, *CTRP5,* and *Mfrp* cDNA fragments into the pZac2.1 plasmid to generate pZac2.1.CMV.huMFRP.SV40, pZac2.1.CMV.huCTRP5.SV40, and pZac2.1.CMV.mMfrp.SV40 plasmids.[14] The AAV vectors were created, packaged, and purified at the Penn Vector Corporation (University of Pennsylvania, PA). AAV-GFP vector were obtained from UNC Vector Core Services (University of North Carolina at Chapel Hill, NC).

***Transduction of AAV vectors* in vitro.** At passage 2, iPS-RPE cells from P1, P2 and wild-type control had been moved in trans-well culture system (Costar, 3460). Wild-type control iPS-RPE cells were divided into 4 wells. iPS-RPE cells from either P1 or P2 were divided into 8 wells, 4 of which received AAV-*MFRP* treatment and 4 served as untreated controls. Two lines of patient-specific iPS-RPE and HEK293 cells also had been grown in 24-well flat dish for AAV-*MFRP* infection.

All cells mentioned above were infected with the AAV-*MFRP* vector at a multiplicity of infection (MOI) of 1×10^4 in serum-free RPE medium.[29] After 24 hours, the virus-containing medium was replaced with fresh RPE medium with 5% serum to continue normal RPE culture. One week later, the steps mentioned above were repeated. Human RPE cells, isolated from an autopsied eye shell, were cultured in 6-well plates and infected with the AAV-*CTRP5* vector at an MOI of 1×10^4 as described above. Wild-type control iPS-RPE cells and human autopsy RPE cells were cultured on cover slip and transduced with the AAV-GFP vector at an MOI of 1×10^4 as described above.

***Transduction of AAV vectors* in vivo.** To test whether AAV2/8(Y733F)-m*Mfrp* can restore vision in $Mfrp^{rd6}/Mfrp^{rd6}$ mice, we injected AAV2/8(Y733F)-m*Mfrp* ($1.23e^{12}$ genome copy/ml) into the subretinal space of the right eye of $Mfrp^{rd6}/Mfrp^{rd6}$ mice at postnatal day 5. Injection of 1 µl of virus particle suspension into the sclera limbus caused an ideal bleb detachment at the retinal site of the injection, as evaluated by postsurgical fundus examination. The left eyes of all mice were left untouched and maintained as a control for experimental analyses. Anesthesia and surgery were performed as previously described.[30]

Proteomic analysis. Shotgun proteomic mass spectrometry-based measurements were performed in triplicate on patient specific iPS-RPE and wild-type control iPS-RPE from P1 and P2. A liquid chromatography-mass spectrometry (LC-MS) approach was used for the relative quantitation and simultaneous identification of proteins from all three samples, including triplicate LC/MS/MS chromatograms (technical replicates) collected for each of the three biological replicates. We used Synapt G2 quadrupole-time-of-flight mass spectrometry (Waters Corporation, Milford, MA) to compare proteome subtraction of iPS-derived RPE cell lines from two *MFRP* mutant patients and one healthy donor. The data were analyzed with a ProteinLynx Global Server and TransOmics software (Waters Corporation).

Cells were lysed in M-PER mammalian protein extraction reagent buffer (cat# 78501; Pierce) with proteinase inhibitor (Roche Diagnostics, IN). Total protein was quantified using a Bio-Rad protein reader. Protein samples (20 µg) were then separated on a 10% Tris–Cl gradient gel and electroblotted onto a nitrocellulose membrane. The membranes were incubated in blocking buffer for 1 hour at room temperature, washed three times in PBS + 0.1% Tween for 5 minutes each, and incubated with primary antibody in blocking buffer overnight at 4 °C. Primary antibodies against the following proteins were used for western blots: RPE65 (mouse monoclonal, 1:2,000, Novus Biologicals, Littleton, CO), BESTROPHIN-1 (rabbit monoclonal, 1:500, Abcam, Cambridge, MA), MITF (mouse monoclonal, 1:500, Abcam), VINCULIN (Rabbit monoclonal, 1:1,000, Abcam), MFRP (goat polyclonal, 1:1,000, R&D, Minneapolis, MN), CTRP5 (goat polyclonal, 1:1,000, R&D), β-actin (mouse monoclonal, 1:2000, Abcam), CRALBP (rabbit polyclonal, 1:400, Santa Cruz, Dallas, TX), and GAPDH (mouse monoclonal, 1:5,000, Abcam). Mouse, rabbit, and goat secondary antibodies were obtained from Santa Cruz and used at a concentration of 1:5,000.

Immunofluorescence. Five antibodies against the pluripotency markers Oct-4, Sox-2, TRA-1-60, SSEA4, and NANOG (all 1:500, ASK-306, Applied StemCell, Menlo Park, CA) were used to characterize the iPS cells reprogrammed from the fibroblasts obtained from two *MFRP*-mutant patients and the healthy donor as described previously.[18] DAPI was used to stain the cell nuclei. To study the change in cell shape between normal and *MFRP* mutant iPS-RPE cells, zonula occludens (ZO)-1 (1:500, 40-2200, Invitrogen Life Technologies, Grand Island, NY) staining was performed on RPE isolated from B6 and $Mfrp^{rd6}/Mfrp^{rd6}$ mice and iPS-RPE derived from two *MFRP* mutant patients before and after AAV2/8-hu*MFRP* treatment. Alexa Fluor 488-conjugated goat antirabbit or Alexa Fluor 555-conjugated goat antimouse IgG (1:1,000, Invitrogen, Life Technologies) antibodies were used as secondary antibodies. Images for staining with all antibodies were obtained using the same settings with a fluorescence microscope (Leica DM 5000 B, Leica Microsystems, Germany).

Phalloidin staining was performed to distinguish the fibers of RPE cells in all iPS-RPE lines. The cells were washed two times with PBS and fixed in 4% paraformaldehyde for 10 minutes at room temperature. After washing with PBS two times, the cells were incubated in 0.1% Triton X-100 and PBS for 5 minutes. After two subsequent washes with PBS, phalloidin staining was performed for 30 minutes at room temperature. The phalloidin staining solution was freshly prepared before use according to the manufacturer's instructions (R415, Invitrogen). The stained cells were observed by confocal microscopy (Zeiss LSM5 Confocal Microscopy, Germany).

Transmission electron microscopy. To monitor apical microvilli of RPE cells, transmission electron microscopy (TEM) was performed on iPS-RPE cells from the two *MFRP*-mutant patients before and after AAV-*huMFRP* treatment. Selected areas were trimmed for ultrathin sectioning and stained with uranyl acetate before visualization by EM.[31]

Measurement of transepithelial resistance. The transepithelial resistance (TER) of confluent, pigmented iPS-RPE monolayers cultured on permeable transwell filters was measured using an epithelial volt-ohm meter (EVOM2) (World Precision Instruments, Sarasota) according to the manufacturer's instructions.[32] For trans-well culture system in this study, there are four wells for each line of P1, P1 after AAV-*MFRP* treated, P2, P2 after AAV-*MFRP* treated and wild-type control. Each well would be measured three times at each time point (weekly). The net TER was calculated by subtracting the background measurement obtained from cell-free, matrigel-coated transwell filters, and then multiplying the difference by the area of the transwell filter to obtain values in Ω/cm^2. The net TER comparison of patient-specific iPS-RPE lines before and after AAV-*MFRP* treated was conducted using ratio paired *t*-test statistical analyses.

Quantitative fundus autofluorescence imaging. Mice were anesthetized with an intraperitoneal injection of ketamine (100 mg/kg) and xylazine (10 mg/kg). Pupils were dilated to an ~2.5 mm (range 2.1–2.9) diameter by administering 1% tropicamide and 2.5% phenylephrine 15 minutes before image acquisition. The fundus was aligned and focused using the near infrared reflectance (NIR-R; 820 nm) mode using high sensitivity to ensure an evenly illuminated fundus, followed by lowering the sensitivity to make the retinal details visible. The retina was then preexposed at 488 nm in AF mode for 20 seconds to bleach the visual pigment. The detector sensitivity was set at an optimal range that was then used for all AF imaging. To determine reproducibility, two images were acquired in each of the two separate sessions. During each session, neither the mouse nor the camera was moved. Between the two sessions, the image was realigned and refocused, and the mouse was repositioned.[33]

Electroretinogram (ERG). ERGs were conducted on $Mfrp^{rd6}/Mfrp^{rd6}$ mice as described previously.[19] All manipulations were conducted under dim red

light, and Espion ERG Diagnosys equipment (Diagnosys LLC, Lowell, MA) was used for the recordings. Adult C57BL/6 (B6) mice were tested at the beginning of each session as controls to ensure both eyes had the same amplitude. Before each ERG recording, *Mfrp*^{rd6}/*Mfrp*^{rd6} mice that were subretinally injected with AAV2/8(Y733F)-m*Mfrp* were dark-adapted for 12 hours and then anesthetized by intraperitoneal injection of 10% ketamine-xylazine-PBS solution. Topical proparacaine and tropicamide (1%) were used for local anesthesia, and phenylephrine (2.5%) was used for pupillary dilation.

Histology and immunofluorescence of the AAV transduced eyes. After subretinal injection of AAV2/8-m*Mfrp*, *Mfrp*^{rd6}/*Mfrp*^{rd6} mice were sacrificed; then, both eyes were enucleated and fixed in 1:2x Karnovsky fixative (2% Paraformaldehyde and 1.5% glutaraldehyde) for 24 hours. The eyes were embedded in paraffin and sectioned. Retinal sections stained with hematoxylin and eosin were visualized by light microscopy (Leica DM 5000B, Leica Microsystems, Germany). Retinal frozen sections stained with *MFRP* antibody and DAPI as mentioned above and were examined by fluorescence microscopy (Leica DM 5000B, Leica Microsystems).

SUPPLEMENTARY MATERIAL

Figure S1. Pedigree of Patient 1.
Figure S2. Phase images and teratoma assay of patient-specific iPS cell lines.
Figure S3. Quantification of RPE markers.
Figure S4. Quantification of MFRP, CTRP5 and β-actin Expression in MFRP-deficient and CTRP5-overexpressed RPE cells.
Figure S5. Images of immunofluorescence on iPS-RPE.
Table S1. Upregulated proteins in patient-specific iPS-RPE involved with actin cytoskeleton.

ACKNOWLEDGMENTS

We thank Sherry Shen, Scott Smemo, Lewis Brown, Kristy Brown, and members of the Bernard & Shirlee Brown Glaucoma laboratories for sharing ideas, cell lines, antisera, and equipment, and for critically reviewing the manuscript, especially, Kelly Davis; and supports from The Macula Foundation Inc, Justin A Manus, Kobi and Nancy Karp. Imaging and animal facilities are supported by the National Institute of Health Core grant 5P30EY019007 and NCI Core grant 5P30CA013696 and unrestricted funds from Research to Prevent Blindness, Columbia University, New York and University of Illinois, Chicago, USA. S.H.T. is a member of the RD-CURE Consortium and is supported by Tistou and Charlotte Kerstan Foundation, NIH R01EY018213, the Research to Prevent Blindness Physician-Scientist Award, the Schneeweiss Stem Cell Fund, New York State (N09G-302 and N13G-275), and the Foundation Fighting Blindness New York Regional Research Center Grant (C-NY05-0705-0312), the Joel Hoffman Fund, Gale and Richard Siegel Stem Cell Fund, Charles Culpeper Scholarship, Laszlo Bito and Olivia Carino Foundation, Irma T. Hirschl Charitable Trust, Bernard and Anne Spitzer Stem Cell Fund, Professor Gertrude Rothschild Stem Cell Foundation, and Gebroe Family Foundation. H.V.N. is supported by the RPB Medical Student Fellowship.

REFERENCES

1. Tsuji, O, Miura, K, Okada, Y, Fujiyoshi, K, Mukaino, M, Nagoshi, N *et al.* (2010). Therapeutic potential of appropriately evaluated safe-induced pluripotent stem cells for spinal cord injury. *Proc Natl Acad Sci USA* **107**: 12704–12709.
2. Yang, J, Li, Y, Chan, L, Tsai, Y, Wu, W, Nguyen, HV *et al.* (2014). Validation of genome-wide association study (GWAS)-identified disease risk alleles with patient-specific stem cell lines. *Hum Mol Gen* **23**: 3445–3455.
3. Singh, R, Shen, W, Kuai, D, Martin, JM, Guo, X, Smith, MA *et al.* (2013). iPS cell modeling of Best disease: insights into the pathophysiology of an inherited macular degeneration. *Hum Mol Genet* **22**: 593–607.
4. Jin, ZB, Okamoto, S, Osakada, F, Homma, K, Assawachananont, J, Hirami, Y *et al.* (2011). Modeling retinal degeneration using patient-specific induced pluripotent stem cells. *PLoS ONE* **6**: e17084.
5. Lustremant, C, Habeler, W, Plancheron, A, Goureau, O, Grenot, L, de la Grange, P *et al.* (2013). Human induced pluripotent stem cells as a tool to model a form of Leber congenital amaurosis. *Cell Reprogram* **15**: 233–246.
6. Katoh, M (2001). Molecular cloning and characterization of MFRP, a novel gene encoding a membrane-type Frizzled-related protein. *Biochem Biophys Res Commun* **282**: 116–123.
7. Zenteno, JC, Buentello-Volante, B, Quiroz-González, MA and Quiroz-Reyes, MA (2009). Compound heterozygosity for a novel and a recurrent MFRP gene mutation in a family with the nanophthalmos-retinitis pigmentosa complex. *Mol Vis* **15**: 1794–1798.
8. Hayward, C, Shu, X, Cideciyan, AV, Lennon, A, Barran, P, Zareparsi, S *et al.* (2003). Mutation in a short-chain collagen gene, CTRP5, results in extracellular deposit formation in late-onset retinal degeneration: a genetic model for age-related macular degeneration. *Hum Mol Genet* **12**: 2657–2667.
9. Kameya, S, Hawes, NL, Chang, B, Heckenlively, JR, Naggert, JK and Nishina, PM (2002). Mfrp, a gene encoding a frizzled related protein, is mutated in the mouse retinal degeneration 6. *Hum Mol Genet* **11**: 1879–1886.
10. Sundin, OH, Dharmaraj, S, Bhutto, IA, Hasegawa, T, McLeod, DS, Merges, CA *et al.* (2008). Developmental basis of nanophthalmos: MFRP Is required for both prenatal ocular growth and postnatal emmetropization. *Ophthalmic Genet* **29**: 1–9.
11. Mandal, MN, Vasireddy, V, Reddy, GB, Wang, X, Moroi, SE, Pattnaik, BR *et al.* (2006). CTRP5 is a membrane-associated and secretory protein in the RPE and ciliary body and the S163R mutation of CTRP5 impairs its secretion. *Invest Ophthalmol Vis Sci* **47**: 5505–5513.
12. Mukhopadhyay, R, Sergouniotis, PI, Mackay, DS, Day, AC, Wright, G, Devery, S *et al.* (2010). A detailed phenotypic assessment of individuals affected by MFRP-related oculopathy. *Mol Vis* **16**: 540–548.
13. Wert, KJ, Sancho-Pelluz, J and Tsang, SH (2014). Mid-stage intervention achieves similar efficacy as conventional early-stage treatment using gene therapy in a pre-clinical model of retinitis pigmentosa. *Hum Mol Genet* **23**: 514–523.
14. Wert, KJ, Davis, RJ, Sancho-Pelluz, J, Nishina, PM and Tsang, SH (2013). Gene therapy provides long-term visual function in a pre-clinical model of retinitis pigmentosa. *Hum Mol Genet* **22**: 558–567.
15. Dinculescu, A, Estreicher, J, Zenteno, JC, Aleman, TS, Schwartz, SB, Huang, WC *et al.* (2012). Gene therapy for retinitis pigmentosa caused by MFRP mutations: human phenotype and preliminary proof of concept. *Hum Gene Ther* **23**: 367–376.
16. Silva, JC, Denny, R, Dorschel, C, Gorenstein, MV, Li, GZ, Richardson, K *et al.* (2006). Simultaneous qualitative and quantitative analysis of the Escherichia coli proteome: a sweet tale. *Mol Cell Proteomics* **5**: 589–607.
17. Fogerty, J and Besharse, JC (2011). 174delG mutation in mouse MFRP causes photoreceptor degeneration and RPE atrophy. *Invest Ophthalmol Vis Sci* **52**: 7256–7266.
18. Li, Y, Tsai, YT, Hsu, CW, Erol, D, Yang, J, Wu, WH *et al.* (2012). Long-term safety and efficacy of human induced pluripotent stem cell (iPS) grafts in a preclinical model of retinitis pigmentosa. *Mol Med* **18**: 1312–1319.
19. Wang, NK, Tosi, J, Kasanuki, JM, Chou, CL, Kong, J, Parmalee, N *et al.* (2010). Transplantation of reprogrammed embryonic stem cells improves visual function in a mouse model for retinitis pigmentosa. *Transplantation* **89**: 911–919.
20. Mandal, MN, Vasireddy, V, Jablonski, MM, Wang, X, Heckenlively, JR, Hughes, BA *et al.* (2006). Spatial and temporal expression of MFRP and its interaction with CTRP5. *Invest Ophthalmol Vis Sci* **47**: 5514–5521.
21. Kishore, U, Ghai, R, Greenhough, TJ, Shrive, AK, Bonifati, DM, Gadjeva, MG *et al.* (2004). Structural and functional anatomy of the globular domain of complement protein C1q. *Immunol Lett* **95**: 113–128.
22. Shu, X, Tulloch, B, Lennon, A, Vlachantoni, D, Zhou, X, Hayward, C *et al.* (2006). Disease mechanisms in late-onset retinal macular degeneration associated with mutation in C1QTNF5. *Hum Mol Genet* **15**: 1680–1689.
23. Chavali, VR, Khan, NW, Cukras, CA, Bartsch, DU, Jablonski, MM and Ayyagari, R (2011). A CTRP5 gene S163R mutation knock-in mouse model for late-onset retinal degeneration. *Hum Mol Genet* **20**: 2000–2014.
24. Ayyagari, R, Mandal, MN, Karoukis, AJ, Chen, L, McLaren, NC, Lichter, M *et al.* (2005). Late-onset macular degeneration and long anterior lens zonules result from a CTRP5 gene mutation. *Invest Ophthalmol Vis Sci* **46**: 3363–3371.
25. Hua, H, Shang, L, Martinez, H, Freeby, M, Gallagher, MP, Ludwig, T *et al.* (2013). iPSC-derived ß cells model diabetes due to glucokinase deficiency. *J Clin Invest* **123**: 3146–3153.
26. Lin, T, Ambasudhan, R, Yuan, X, Li, W, Hilcove, S, Abujarour, R *et al.* (2009). A chemical platform for improved induction of human iPSCs. *Nat Methods* **6**: 805–808.
27. Idelson, M, Alper, R, Obolensky, A, Ben-Shushan, E, Hemo, I, Yachimovich-Cohen, N *et al.* (2009). Directed differentiation of human embryonic stem cells into functional retinal pigment epithelium cells. *Cell Stem Cell* **5**: 396–408.
28. Maminishkis, A, Chen, S, Jalickee, S, Banzon, T, Shi, G, Wang, FE *et al.* (2006). Confluent monolayers of cultured human fetal retinal pigment epithelium exhibit morphology and physiology of native tissue. *Invest Ophthalmol Vis Sci* **47**: 3612–3624.
29. Vasireddy, V, Mills, JA, Gaddameedi, R, Basner-Tschakarjan, E, Kohnke, M, Black, AD *et al.* (2013). AAV-mediated gene therapy for choroideremia: preclinical studies in personalized models. *PLoS ONE* **8**: e61396.
30. Davis, RJ, Tosi, J, Janisch, KM, Kasanuki, JM, Wang, NK, Kong, J *et al.* (2008). Functional rescue of degenerating photoreceptors in mice homozygous for a hypomorphic cGMP phosphodiesterase 6 b allele (Pde6bH620Q). *Invest Ophthalmol Vis Sci* **49**: 5067–5076.
31. Tsang, SH, Gouras, P, Yamashita, CK, Kjeldbye, H, Fisher, J, Farber, DB *et al.* (1996). Retinal degeneration in mice lacking the gamma subunit of the rod cGMP phosphodiesterase. *Science* **272**: 1026–1029.
32. Sonoda, S, Spee, C, Barron, E, Ryan, SJ, Kannan, R and Hinton, DR (2009). A protocol for the culture and differentiation of highly polarized human retinal pigment epithelial cells. *Nat Protoc* **4**: 662–673.
33. Sparrow, JR, Blonska, A, Flynn, E, Duncker, T, Greenberg, JP, Secondi, R *et al.* (2013). Quantitative fundus autofluorescence in mice: correlation with HPLC quantitation of RPE lipofuscin and measurement of retina outer nuclear layer thickness. *Invest Ophthalmol Vis Sci* **54**: 2812–2820.